Functional Assessment of Metal Oxide Nanoparticle Toxicity in Immune Cells

Melissa A. Maurer-Jones, Yu-Shen Lin, and Christy L. Haynes*

Department of Chemistry, University of Minnesota, 207 Pleasant Street SE, Minneapolis, Minnesota 55455

There is currently significant worldwide effort to fabricate and characterize novel nanoscale materials, and as researchers vary the chemical composition, size, shape, and assembly of nanoparticles, the potential applications seem endless based on the novel size-dependent chemical and physical properties. With this intense focus on nanomaterial development, there has been a boom in the number of consumer products commercially available that exploit nanoscience. Concurrently, the field of nanotoxicology has emerged in an effort to understand the interaction of nanomaterials with the environment and human physiology so that this technology can be used with minimal risk.

Nanotoxicology faces many challenges as nanoparticles, with many novel properties, are placed into complex, dynamic biological systems.[1,2] One challenge is the limitation in technology to characterize nanoparticles throughout their interaction with the biological system and to accurately quantify nanoparticle uptake location and concentration. Additionally, while a myriad of *in vivo* and *in vitro* nanotoxicity assessments have been performed to characterize the toxicology of engineered nanoparticles,[1-3] many of the assessment methods were designed to study molecular toxicants, which likely have different cellular interactions than nanoparticles. The *in vitro* toxicity assays that are often employed for these studies do not necessarily accurately predict *in vivo* response,[4,5] and they may fail in the presence of nanoparticles.[6-8] To overcome these limitations and gain a deeper understanding of nanoparticle—cell interactions, we have employed carbon-fiber microelectrode amperometry (CFMA) to explore fundamental

ABSTRACT Understanding the nanoparticle—cell interaction is critical for the safe development of nanomaterials. Herein, we explore the impact of three metal oxide nanoparticles, nonporous Stöber SiO_2, mesoporous SiO_2, and nonporous anatase TiO_2 nanoparticles, on primary culture mast cells. Using transmission electron microscopy and inductively coupled plasma atomic emission spectroscopy, we demonstrate that each class of nanoparticle is internalized by the mast cells, localizing primarily in the secretory granules, with uptake efficiency increasing in the following order: nonporous SiO_2 < porous SiO_2 < nonporous TiO_2 nanoparticles. The influence of nanoparticle-laden granules was assessed using carbon-fiber microelectrode amperometry measurements that reveal functional changes in chemical messenger secretion from mast cell granules. Both nonporous and porous SiO_2 nanoparticles cause a decrease in the number of molecules released per granule, with nonporous SiO_2 also inducing a decrease in the amperometric spike frequency and, therefore, having a larger impact on cell function. As the two classes of SiO_2 nanoparticles vary only in their porosity, these results suggest that, while the mesoporous SiO_2 has a drastically larger total surface area due to the pores, the cell-contactable surface area, which is higher for the nonporous SiO_2, is more important in determining a nanoparticles' cellular impact. In comparison, exposure to nonporous TiO_2 slows the kinetics of secretion without altering the number of molecules released from the average granule. The varying immune cell response following exposure to nonporous SiO_2 and nonporous TiO_2 indicates that the nanoparticle—cell interactions are also modulated by surface chemistry.

KEYWORDS: silica · titania · nanotoxicity · amperometry · mesopore · surface area · surface chemistry

questions regarding the impact of nanoparticles on the critical cell function of exocytosis.[9,10] During exocytosis, a highly conserved cellular function across cell types and species, intracellular granules fuse with the plasma membrane and the granule contents are released, enabling communication between cells through secreted chemical messengers.[11] CFMA is a single-cell analysis technique that reveals a wealth of information regarding the biophysics of exocytosis, and accordingly, changes in this critical cell function should nanoparticles interfere with any components of the exocytotic machinery.

One cell type well-known for exocytotic delivery of chemical messengers is the mast cell. Mast cells are found in many tissues

*Address correspondence to chaynes@umn.edu.

TABLE 1. Nanoparticle Characteristics

nanoparticle	size (nm)	total surface area (m²/g)	pore volume (cm³/g)	ζ-potential (mV)	crystallinity
nonporous SiO₂	24 ± 3	127		−28.16	amorphous
porous SiO₂	25 ± 4	1164	0.92	−16.94	amorphous
nonporous TiO₂	11 ± 5	234		−13.58	93.5% anatase 6.5% brookite

of the body and play a critical role in immune response,[12,13] making them a good model for nanotoxicity studies. To mimic an *in vivo* response with the *in vitro* CFMA assay, we have chosen to co-culture primary murine peritoneal mast cells (MPMCs) with Swiss albino fibroblasts (3t3).[9,10] Not only does this co-culture better simulate multicellular tissue, but it has also been demonstrated that the MPMC/3t3 co-culture allows the primary culture MPMCs to secrete more chemical messenger molecules and maintain their exocytotic cell function in culture for up to a month.[14]

While nanoscale particles can be fabricated with diverse elemental compositions, metal oxide nanoparticles are of particular importance based their widespread use in a variety of crystalline forms. Specifically, silica (SiO_2) and titania (TiO_2) nanoparticles are the focus of this work because they are two of the most commonly used materials in commercially available products,[15] and both nanoparticles are the focus of much forward-looking research as well. SiO_2, used as an additive in various commercially available products, has also become a critical nanoparticle in biomedical and biotechnological fields. Particular attention has been paid to mesoporous SiO_2 composites because of their potential as a multifunctional template for diagnosis, imaging, targeting, and drug delivery.[16−18] The porosity of these particles drastically increases the total surface area, allowing for the presence of more reactive surface atoms that have the potential to contribute to cytotoxicity. Within the nanotoxicology community, surface reactivity is of great concern as it is proposed to be a major cause of toxic response, likely through the production of reactive oxygen species.[19,20] While it is thought that an increased surface area indicates an increase in surface reactivity because there are more surface atoms available to react with cells or the environment, there have been limited studies that directly monitor the impact that highly porous structures have on the toxicity of the nanoparticle.[21−24] Herein, we aim to understand the nanoparticle−cell interactions of the porous particles as compared to their nonporous counterparts by exposing immune system cells to Stöber and mesoporous SiO_2 of similar diameter.

The composition and crystallinity of a nanoparticle are also likely to influence impacts on cell health. To shed light on these effects, the biophysical ramifications of SiO_2 nanoparticles on exocytotic behavior were compared to those of another metal oxide, TiO_2. TiO_2 is commonly found in cosmetics,[25] including sunscreen,

and has proven to be a particularly promising technology as a photocatalyst in pollutant remediation[26,27] and photoactive material in solar cells.[28,29] *In vitro* studies using traditional toxicological assays have shown that nanoscale TiO_2 induces oxidative stress, with anatase having larger impacts than rutile, decreasing cellular viability and causing cell death.[30−32] Herein, we will compare the impact of anatase TiO_2 nanoparticles on cellular exocytosis to the effects of the aforementioned SiO_2 material.

This work demonstrates that MPMCs differentially internalize nanoparticles with different porosities and composition and experience variation in extent of toxicity, as confirmed using traditional toxicological assays. Using CFMA on nanoparticle-exposed MPMC/3t3 co-culture, we reveal new insights regarding the biophysical impact of nanoparticles with varying porosity and material on exocytotic cell function of MPMCs, illuminating details about how a surviving cell adapts to the presence of metal oxide nanoparticles.

RESULTS AND DISCUSSION

Nanoparticle Characterization. Nonporous SiO_2, porous SiO_2, and nonporous TiO_2 were synthesized and then characterized using transmission electron microscopy (TEM), X-ray diffraction (XRD), ζ-potential analysis, and nitrogen adsorption-desorption isotherms, with results summarized in Table 1. On the basis of TEM analysis (Figure 1), nonporous and porous SiO_2 are 24 ± 3 (*n* = 220) and 25 ± 4 nm (*n* = 250) in diameter, respectively, whereas the nonporous TiO_2 particles are 11 ± 5 nm (*n* = 306). While it would be ideal, for comparison purposes, for the nonporous SiO_2 and TiO_2 to be the same size, it is difficult to maintain the monocrystallinity of TiO_2 nanoparticles when they are larger than ∼12 nm diameter.[33] The state of nanoparticle−nanoparticle association ahead of cell interaction is likely critical in determining extent of uptake. Herein, nanoparticles are considered to be agglomerated if they experience reversible adhesion, whereas aggregation is considered to be the irreversible bonding of nanoparticles. On the basis of sonication of nanoparticle suspensions leading to a disassembly of nanoparticle groupings, it can be assumed that the studied nanoparticles are reversibly agglomerated. It is evident from Figure 1C and dynamic light scattering measurements (see Table S1 in Supporting Information) that the TiO_2 nanoparticles tend to agglomerate more than either class of SiO_2 nanoparticles (Figure 1A,B); among the silica nanoparticles, the light
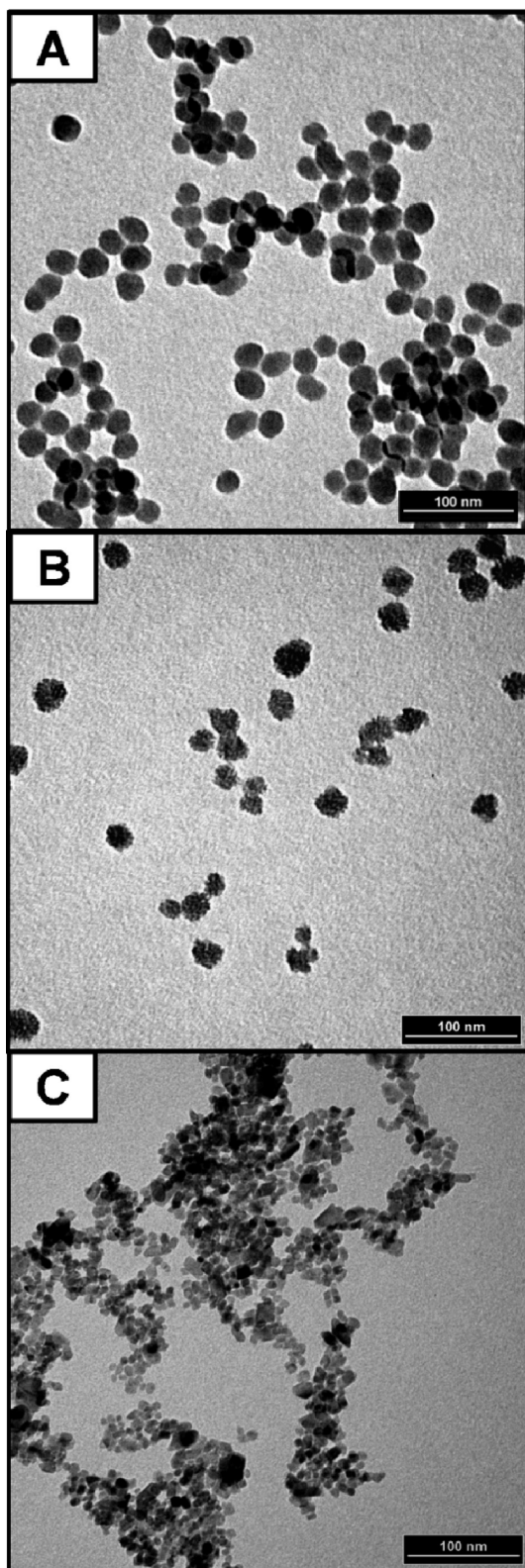
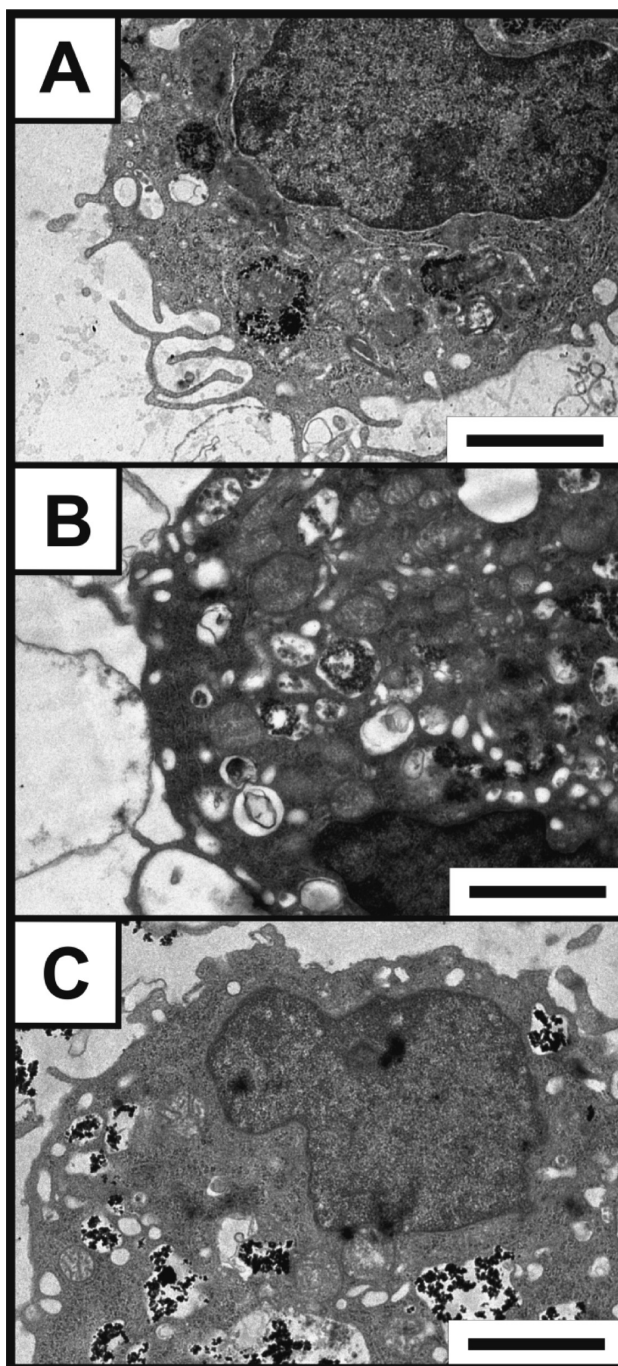Figure 1. TEM images of (A) Stöber nonporous SiO₂, (B) porous SiO₂, and (C) nonporous TiO₂.

Figure 2. TEM images of MPMCs used in experiments showing nanoparticle uptake after 24 h exposure to 100 μg/mL of (A) nonporous SiO₂, (B) porous SiO₂, and (C) nonporous TiO₂ nanoparticles. Nanoparticles appear to localize within the granules. Each scale bar = 2 μm.

scattering measurements indicate that porous SiO₂ agglomerates slightly more than nonporous SiO₂. Although it is common for these nanomaterials to be synthesized as aggregates, this study deliberately did not

control this aggregation state because it reflects more relevant conditions of industrially produced material. The XRD analysis of crystallinity showed that the nonporous and porous SiO₂ particles are amorphous, but the nonporous TiO₂ particles are crystalline, with 93.5% anatase and 6.5% brookite composition, as determined by the Rietveld method of refinement.[34] Using Brunauer-Emmet-Teller (BET) modeling of nitrogen

adsorption-desorption isotherms (see Supporting Information Figure S1) to determine total nanoparticle surface area, the porous SiO_2 nanoparticles have a considerably higher surface area (1164 m^2/g) than the nonporous SiO_2 (127 m^2/g). The increased surface area can be attributed to the porous nature of the nanoparticles; however, the majority of the surface area in the porous nanoparticles is on the inside of the cylindrical pores, and therefore, there is a limited contactable surface area for cell-bound molecules and proteins to interact. In fact, since the nonporous and porous SiO_2 are of similar size, it can be assumed that the nonporous SiO_2 has a greater external surface that is accessible to cells than the porous nanoparticles because the pores decrease the external surface area.[24] The calculated surface area of the nonporous TiO_2 was 234 m^2/g and presents a solid surface comparable to the nonporous SiO_2, facilitating comparison between the effects of SiO_2 and TiO_2 surfaces. All ζ-potentials were negative, indicating relative stability within a suspension. TiO_2 has the lowest magnitude ζ-potential, which is consistent with TiO_2 nanoparticles having the greatest extent of agglomeration, followed by porous SiO_2 and then nonporous SiO_2. Because all three classes of nanoparticles have a ζ-potential with smaller magnitude than -30 mV, they are considered to have a similar relative stability,[35] making aggregation state an unlikely determinant of cellular toxicity. While the aforementioned characteristics are the best estimate of the state of the nanoparticles as "seen" by the cells, it is likely that the surface of the nanoparticle will change *en route* to and following cellular uptake.[19,36]

Nanoparticle Uptake. To accurately assess nanoparticle impact on cell function, it is essential to first characterize the internalization of nanoparticles. In the literature, nanoparticle uptake has been shown to depend on nanoparticle size and surface chemistry.[37−39] Herein, TEM was employed to qualitatively characterize nanoparticle uptake, while atomic emission spectroscopy (ICP-AES) was used to quantify nanoparticle uptake. Using TEM after a 24 h exposure to 100 μg/mL of nanoparticles, the nanoparticles are apparent within the cell regardless of the particle type and generally seen localized within the secretory granules of the MPMCs (Figure 2). On the basis of the TEM images, neither nonporous nor porous SiO_2 nanoparticles tend to agglomerate outside the cell during uptake; however, the TiO_2 nanoparticles are seen both inside and outside the plasma membrane in agglomerates of tens of nanoparticles. Qualitatively, the TEM images of nonporous TiO_2 uptake indicate that about half of the nanoparticles are taken up by the MPMCs. Because sectioned TEM images are not appropriate for quantitation, the complementary technique of ensemble-averaged atomic spectroscopy has also been employed herein.

ICP-AES allows for quantification of cellular nanoparticle uptake by detection of titanium or silicon atomic emission, which can be converted to the number of nanoparticles internalized by each cell as described in the Methods and Supporting Information. From the results shown in Table 2, where cells were exposed to nanoparticles in varying concentrations (100 and 200 μg/mL) for 24 h, we observed that cells take up significantly ($p < 0.05$) more nanoparticles when exposed to higher concentrations. It follows that decreasing the exposure concentration would likely yield a decrease in the number of nanoparticles internalized by the cells. This supports many literature examples where an increase in nanoparticle dose has a greater influence on cell function and viability.[21,22,40] The ICP-AES data also reveal that nanoparticles are internalized differently based on the type of nanoparticle. It is readily apparent that mesoporous SiO_2 is more efficiently incorporated into cells than its nonporous counterpart of the same size, potentially due to a higher degree of agglomeration. This result is similar to a recently published paper where the authors showed that mesoporous SiO_2 nanoparticles exhibited higher cellular labeling efficacy than nonporous SiO_2 nanoparticles.[41] In addition, it appears that the smaller diameter and higher degree of agglomeration of the TiO_2 nanoparticles facilitate more extensive interaction with the cells than either of the SiO_2 nanoparticle classes; however, because ICP-AES data do not reveal nanoparticle localization within a cell, much of this could be due to extracellular adhesion rather than internalization. Even if, as indicated by TEM, half of the TiO_2 nanoparticles are outside the cell, TiO_2 uptake is still more efficient than either of the SiO_2 nanoparticle classes considered at both 100 and 200 μg/mL concentrations ($p < 0.05$). The combined picture of TEM-based localization information and ICP-AES nanoparticle count reveals important trends about cellular uptake of nanoparticles in and of itself. More important to this work, however, is the ability to correlate nanoparticle uptake with both cell viability and cell function.
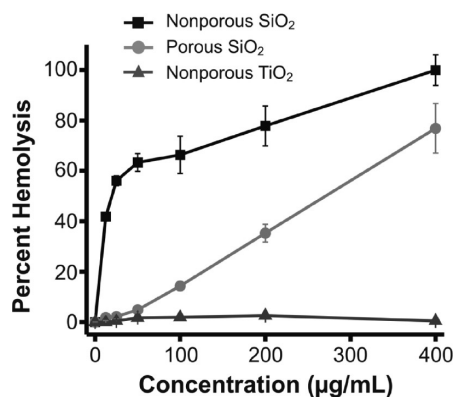
TABLE 2. ICP-AES Uptake Data in MPMCs after 24 h Exposure to 100 and 200 μg/mL Nonporous SiO_2, Porous SiO_2, and Nonporous TiO_2[a]

nanoparticle	100 μg/mL dose (nanoparticles/cell)	200 μg/mL dose (nanoparticles/cell)
nonporous SiO_2	4.5×10^4	1.1×10^7
porous SiO_2	2.0×10^5	3.5×10^7
nonporous TiO_2	7.2×10^7	1.5×10^8

[a]All nanoparticle types are internalized significantly different than the others ($p < 0.05$), and MPMCs internalize nanoparticles at 100 μg/mL significantly less than when cells are exposed to 200 μg/mL ($p < 0.05$).

Figure 3. Hemolysis after 3 h exposure to varying concentrations of nonporous SiO_2, porous SiO_2, and nonporous TiO_2 nanoparticles. Both nonporous and porous SiO_2 nanoparticles cause a concentration-dependent lysis of RBCs. Nonporous TiO_2 exhibits minimal to no hemolysis in RBCs ($n = 3$).

Effects of Porosity and Surface Area. Studies have shown that mesoporous SiO_2 induces varying degrees of toxicity. That is, *in vitro* viability assays have shown decreased cell viability upon exposure to mesoporous SiO_2.[21−23] It has also been demonstrated that mesoporous SiO_2 inhibits cellular and mitochondrial respiration[42] and causes oxidative stress within the exposed cells.[43] To our knowledge, however, these studies have not isolated the variable of porosity on the effects of toxicity and therefore are missing important information on a nanoparticle class with growing use.

To examine the impact of nanoparticle porosity on cellular toxicity, the mast cells were exposed to one of two types of SiO_2 nanoparticles, where the only significant difference between the types was the porosity. Overall viability was measured by monitoring hemolysis of isolated human red blood cells (RBCs) as well as mitochondrial activity in mast cells. The hemolysis behavior (Figure 3) is significantly different, with the nonporous SiO_2 particles damaging RBCs at much lower
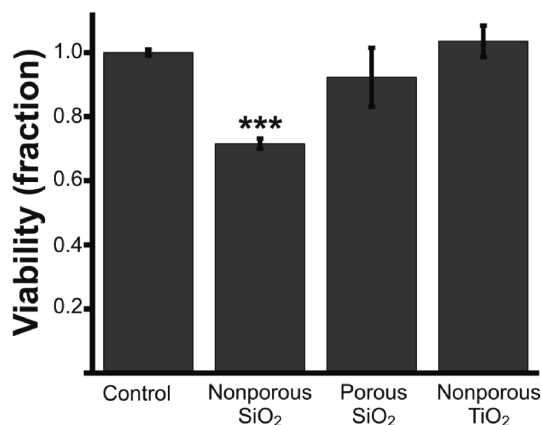

Figure 4. MPMC/3t3 cell viability, as measured with the MTT assay, following exposure to different conditions: control, 100 μg/mL nonporous SiO_2 nanoparticles, 100 μg/mL porous SiO_2 nanoparticles, and 100 μg/mL nonporous TiO_2 nanoparticles for 24 h; *** indicates $p < 0.005$ ($n = 4$) compared to the control ($n = 4$).
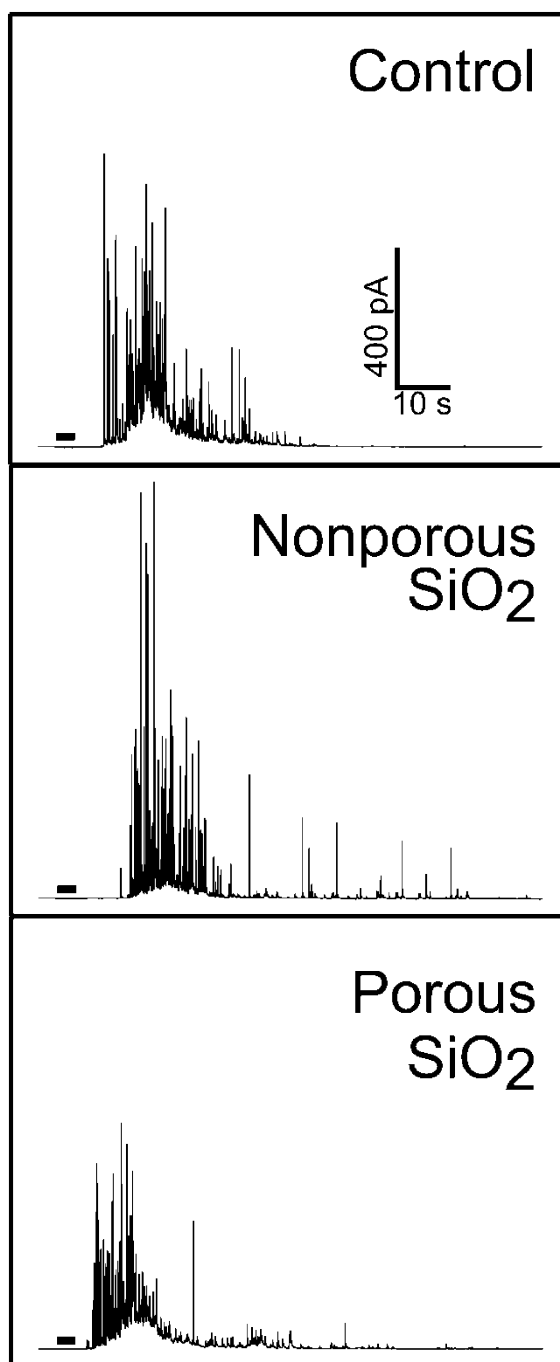

Figure 5. Representative amperometric traces from MPMCs co-cultured with 3t3 fibroblast following exposure to different conditions: control, 100 μg/mL nonporous SiO_2 nanoparticles, and 100 μg/mL porous SiO_2 nanoparticles for 24 h. The bold line on each trace indicates the three second bolus of stimulant delivered to the cell. Traces were chosen that best represented averages per condition.

concentrations than their porous counterparts. In fact, 50% hemolysis requires 270 μg/mL porous SiO_2 but only 20 μg/mL nonporous SiO_2. Similarly, the MTT (3-(4,5-dimethylthiazol-2-yl)-2,5-diphenyltetrazolium bromide) viability assay reveals that porous SiO_2 nanoparticles do not influence mast cell viability (compared to control cells) but that cell viability drops significantly to 72% in the presence of nonporous SiO_2 of the same
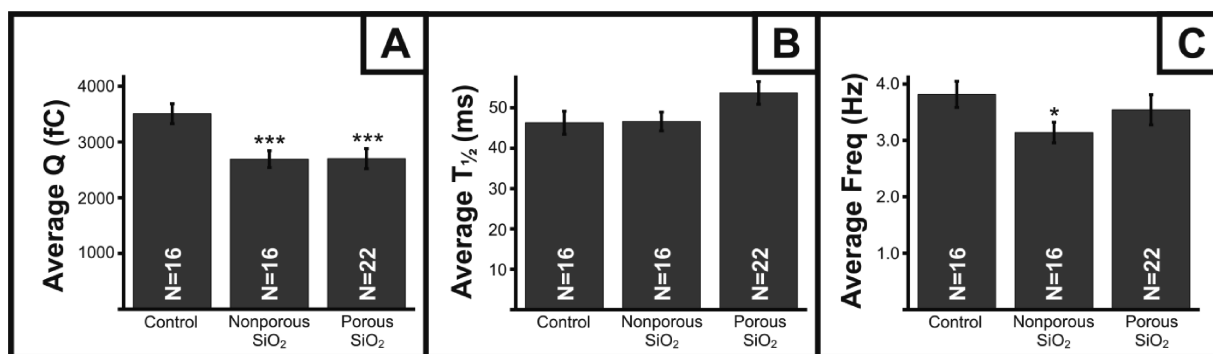
Figure 6. Average amperometry spike parameters from MPMCs in a co-culture with fibroblasts after 24 h exposure to control conditions, 100 μg/mL nonporous SiO_2 nanoparticles, and 100 μg/mL porous SiO_2 nanoparticles. (A) Exposure to both nonporous and porous SiO_2 nanoparticles causes a decrease in average spike area (Q) as compared to control conditions but (B) does not affect the average half-width ($t_{1/2}$) of the amperometric spikes. (C) Nonporous SiO_2 causes a decrease in frequency of spike release as compared to the control. Error bars represent SEM, * indicates $p < 0.05$, and *** indicates $p < 0.005$.

dose (100 μg/mL) (Figure 4). In both cases, it is clear that at least a portion of the mast cells survive nanoparticle exposure for functional assessment.

To reveal potential functional changes in surviving nanoparticle-exposed mast cells, real-time measurement of exocytotic function was performed following cell exposure to either porous or nonporous SiO_2 nanoparticles. Representative amperometric traces from the MPMC/3t3 co-culture can be seen in Figure 5. Analyzing the spike parameters, it is clear that both nonporous and porous SiO_2 cause a decrease in amperometric spike area (Figure 6A). That is, there is a 23 and 22% decrease in the number of molecules released from an average granule during MPMC exocytosis when exposed to nonporous and porous SiO_2 nanoparticles, respectively. This difference corresponds to a drop from an average of 1.09×10^7 serotonin molecules per granule to 8.40×10^6 and 8.42×10^6 serotonin molecules per granule, respectively. Interestingly, the porous and nonporous SiO_2 nanoparticle-exposed cells are not distinguishable from one another ($p > 0.05$) in regard to the number of chemical messenger molecules released, suggesting that it is the nanoparticle itself, not the porosity, that induces a change in chemical messenger storage/delivery. While neither nonporous nor porous SiO_2 nanoparticles significantly alter the kinetics of individual granule fusion or molecule secretion (*i.e.*, no significant change in the $t_{1/2}$; Figure 6B), the nonporous particles do cause a significant alteration to the frequency of granule release (decrease of 18%) as compared to the control (Figure 6C), indicating some disruption of granule trafficking, docking, or lipid membrane fusion that is avoided when mesoporous nanoparticles are used instead. While this characteristic of depressed molecular secretion is similar to that measured in previous work with Au nanoparticle-exposed mast cells,[10] the lack of a correlated change in kinetics suggests that the presence of SiO_2 nanoparticles influences the serotonin content of the granule rather than the heparin proteoglycan sulfate matrix's

ability to unfold and release the serotonin. In addition, the alteration of secretion frequency suggests that nonporous SiO_2 nanoparticles interfere with the cytoskeletal machinery, fusion machinery, or membrane characteristics; this interference is unprecedented in measurements made using Au nanoparticles. Therefore, it is clear that nonporous SiO_2 particles have an overall greater impact on the cell function of MPMCs than either their porous counterpart or nonporous Au nanoparticles of similar size. These data suggest that both surface chemistry and surface area influence nanoparticle toxicity. Surface area is generally considered to be one of the greatest contributors to nanoparticle toxicity with an oft made simple assumption that larger surface area leads to more toxicity;[44,45] however, the results presented herein indicate that porous particles, with large internal surface areas, defy this trend. The more relevant measure is cell-contactable surface area, or the area with which cell membrane, cell-bound proteins, and cell-associated molecules can interact. While small, liberated proteins and molecules may adsorb within the nanoparticle, only cell-bound species are of interest in this case because they are involved directly in the exocytosis function. For these cell-bound species to adsorb into the pores of the mesoporous SiO_2, the nanoparticle and cell would have to align perfectly, and even then, the contactable surface by these species is minimal. Therefore, it appears that the greater external, cell-contactable surface area of the nonporous SiO_2 yields a greater impact on cellular function. A comparison of the hemolytic activity between nonporous and porous SiO_2 nanoparticles of varying size also concludes that nanoparticle toxicity correlates to the cell-contactable surface area as opposed to total surface area.[46]

Material Effects. On the basis of the apparent differences between the Au nanoparticles explored in previous work[9,10] and the SiO_2 nanoparticles included herein, a similar set of analyses were also employed to further explore the impact of nanoparticle composition on cell
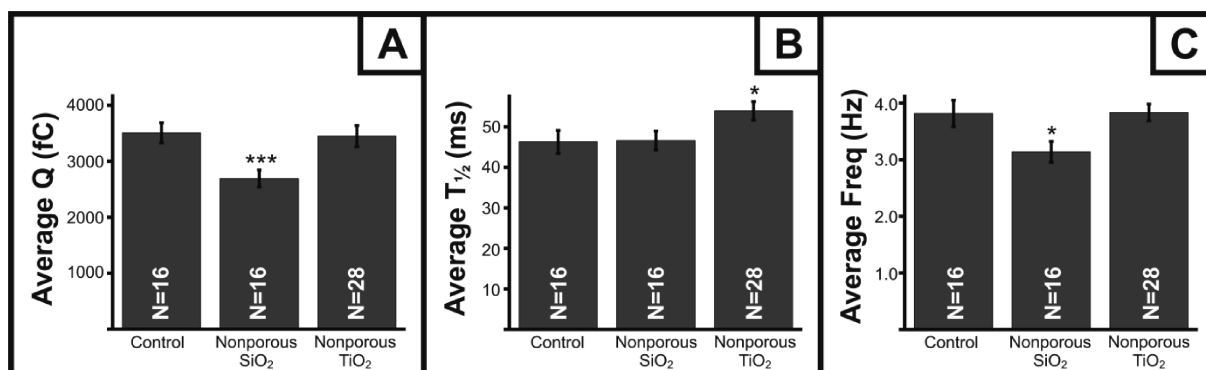
Figure 7. Average amperometry spike parameters for MPMC/3t3 co-culture after exposure to control conditions, 100 μg/mL nonporous SiO_2 nanoparticles, and 100 μg/mL nonporous TiO_2 nanoparticles. (A) Nonporous SiO_2 nanoparticles cause a decrease in the spike area (Q) as compared to the control, whereas nonporous TiO_2 does affect the number of molecules released. (B) Nonporous TiO_2 significantly increases the average half-width ($t_{1/2}$) of spikes, but nonporous SiO_2 does not as compared to the control. (C) Nonporous SiO_2 significantly decreases the average spike frequency as compared to the control. Error bars represent SEM, * indicates $p < 0.05$, and *** indicates $p < 0.005$.

function with crystalline TiO_2 nanoparticles. It can be seen from the hemolysis assay (Figure 3) that nonporous SiO_2 nanoparticles cause the greatest percentage of RBC lysis and nonporous TiO_2 particles demonstrate almost no impact on RBCs. The difference in hemolytic activity between nonporous SiO_2 and nonporous TiO_2 is an early indicator that the material in contact with the cell plays a critical role in toxicity. The MTT assay was performed on the MPMC/3t3 co-culture following TiO_2 exposure (Figure 4), and the results reveal that nonporous TiO_2 nanoparticles do not affect the viability of the cells, despite the significantly enhanced cellular uptake of the smaller TiO_2 nanoparticles compared to the larger SiO_2 nanoparticles. However, in a comparison between nonporous amorphous SiO_2 and nonporous crystalline TiO_2, we see different effects on the biophysics of exocytosis in a MPMC/3t3 co-culture after 24 h exposures at the same mass concentration. Figure 7A shows that SiO_2 causes a significant decrease in Q or the number of molecules released, but Q is maintained after exposure to TiO_2 as compared to the control. Conversely, TiO_2 causes a 17% slowing in the kinetics of chemical messenger release (i.e., larger $t_{1/2}$), as can be seen in Figure 7B, whereas SiO_2 does not alter this biophysical property. This change in kinetics of secretion may be due to the fact that TiO_2 has a higher affinity for protein adsorption than SiO_2,[47] and since MPMC granules contain many proteinaceous mediators,[48] internalized TiO_2 delays content release from the granules. It also appears, based on the unchanging granular secretion frequency (Figure 7C), that the TiO_2 nanoparticles do not alter the cellular machinery that controls granule transport, docking, or fusion unlike their nonporous SiO_2 counterparts. On the basis of the varying biophysical response from MPMC/3t3 co-culture, it can be concluded that the mechanism of interaction between nanoparticles and cells is dependent on the material, which has been implicated in other studies.[49,50] This difference likely arises from the difference in surface chemistry be-

tween particles of different composition, due in part to the surface species (hydroxyl/water groups for TiO_2[51,52] and silanol for SiO_2[53]), the surface atoms (Ti or Si), and the structure in which they are present on the surface of nanoparticles (highly ordered for anatase crystals and amorphous in the case of SiO_2). More work is being pursued on a variety of other materials with systematically varied properties in order to arrive at more generalizable conclusions about the toxicity of nanomaterials. Toward this goal, work will be aimed at understanding the mechanism of impact the nanoparticles have on cell function, such as determining the concentration of reactive oxygen species present upon nanomaterial exposure.

CONCLUSIONS

Safe implementation of nanotechnology requires an intimate understanding of biological materials interactions. A significant portion of nanotoxicology effort has focused only on *in vitro* cell survival following nanomaterial exposure. The work presented herein goes one major step further, examining cell function in cells that have survived the internalization of metal oxide nanoparticles. With an *in vitro* MPMC/3t3 co-culture, we have demonstrated that nonporous SiO_2, porous SiO_2, and nonporous TiO_2 are internalized by the cells and interfere with cell function. From CFMA results, nonporous SiO_2 causes the greatest impact on exocytotic cell function through a decrease in molecules released per exocytotic granule and a decrease in the frequency of release as compared to porous SiO_2. Common viability assays support this trend as both MTT and hemolysis assays show nonporous SiO_2 having a greater impact on cells. Our results indicate that, while other properties may have toxic impacts, a major feature in predicting nanoparticle toxicity is the external surface area of the nanoparticle, and that while porous SiO_2 are more readily taken up by cells, there is less cell-contactable reactive surface area to perturb cell function.

Not only is the area of reactive surface available important for understanding nanoparticle toxicity, but our results suggest that the surface chemistry is also critical in determining the nanoparticle−cell interaction. That is, SiO_2 causes significant impact on cell viability and hemolysis as well as disturbing the exocytotic cell function. Interestingly, however, while TiO_2 does not appear to affect the toxicity as predicted with the traditional ensemble assays, it is internalized by cells and causes changes in the exocytotic cell function. In addition to supporting the role of surface chemistry in determining the nanoparticle−cell interaction, these data support the need for alternative methods of assessing cellular impact of nanoparticles as the bulk assays did not reveal the altered cell function. Along with developing CFMA as a toxicological tool, continued work is needed to understand the causes of change in exocytotic cell function so that we may better control nanoparticle toxicity.

METHODS

Nanoparticle Fabrication. *Stöber Nonporous SiO_2 Nanoparticles:* Nonporous SiO_2 nanoparticles were synthesized using a modified Stöber method[54] as shown in related work.[55] Briefly, 0.75 mL of 28−30% ammonium hydroxide (Mallinckrodt, Phillipsburg, NJ) was added to 40 mL of 95% ethanol (Pharmco-Aaper, Brookfield, CT) held at 40 °C, followed by the addition of 0.5 mL of tetraethyl orthosilicate (TEOS) (Sigma-Aldrich, Milwaukee, WI). The mixture was continuously stirred at 40 °C for 12 h to form the ultrafine SiO_2 nanoparticles. The nanoparticles were purified through centrifugation, rinsed with ethanol between centrifugation steps, and finally stored in ethanol. Nanoparticles were rinsed and resuspended in calcium- and magnesium-free PBS (Sigma-Aldrich, Milwaukee, WI) for at least a week prior to exposure.

Mesoporous SiO_2 Nanoparticles: Porous SiO_2 nanoparticles were prepared in highly dilute and base-catalyzed conditions as described in a recently published paper.[46] Typically, 0.29 g of *n*-cetyltrimethylammonium bromide (CTAB, 99%) was dissolved in 150 mL of 0.128 M ammonium hydroxide solution at 60 °C. Then, 2.0 mL of 0.88 M ethanolic TEOS was added to the solution under vigorous stirring (600 rpm). After 1 h, the mixture solution was aged for another 12 h. The as-synthesized colloids were transferred to 50 mL of ethanolic ammonium nitrate solution (6 g/L) and kept under stirring at 60 °C for 1 h to remove surfactants. The surfactant extraction step was repeated twice. The extracted nanoparticles were washed with ethanol twice and suspended in absolute ethanol. Nanoparticles were transferred and resuspended in PBS for a minimum of a week prior to exposure.

Nonporous TiO_2 Nanoparticles: Nanoparticles were synthesized in an acid-catalyzed sol−gel synthesis as described previously by Isley and Penn.[56] Briefly, 125 mL of isopropyl alcohol (BDH, West Chester, PA) and 12.5 mL titanium(IV) isopropoxide (Sigma-Aldrich, Milwaukee, WI) were stirred in an ice bath for 30 min after which 7.4 mL of 3.2 M nitric acid (BDH, West Chester, PA) was added dropwise. The mixture was allowed to come to room temperature and then refluxed for 24 h. The as-synthesized nanoparticle suspension was dialyzed in regenerated cellulose tubing (nominal MWCO 3500, Fisher Scientific, Pittsburgh, PA) against Milli-Q purified water (Millipore Corporation, Burlington, MA) for 5 days, changing the water at least 10 times. Following dialysis, an aliquot of nanoparticle suspension was placed in an acid digestion bomb with water (3:5 nanoparticle suspension/Milli-Q water) and put in a 200 °C oven for 48 h.

Nanoparticle Characterization. *TEM:* Transmission electron microscope (TEM) images were taken on a JEOL 1200 EXII (JEOL, Tokyo, Japan) at 100 kV. Specimens were prepared by evaporating one drop of ethanolic nanoparticle solution on a Formvar-coated copper grid (Ted Pella, Redding, CA).

XRD: Powder X-ray diffraction (XRD) for porous SiO_2 was performed on a Bruker-AXS D-5005 (Siemens) with Cu Kα radiation at 45 kV and 40 mA. Spectra were collected from 1.5 to 8° by step scan with a step size of 0.04° and a dwell time of 1.0 s. XRD of TiO_2 was performed on a PANalytical X'Pert Pro diffractometer (Almelo, The Netherlands) with a high speed X'Celerator detector and a Co Kα radiation source at 45 kV and 40 mA. Spectra were collected from 25 to 95° by continuous scan with a step size of 0.017° and a dwell time of 250 s. TiO_2 phase compositions were determined by the Rietveld method[34] using X'Pert High Score Plus (version 2.0.1) software (PANalytical, Almelo, The Netherlands) and the known crystal structures of anatase, brookite, and rutile as starting points. The parameters that were refined were the scale factor, specimen displacement, background, unit cell parameters, extinction coefficients, preferred orientation, and W, U, and V profile parameters.

Zeta-Potential Analysis: Nonporous SiO_2, porous SiO_2, and nonporous TiO_2 were suspended in PBS (Sigma-Aldrich, Milwaukee, WI) at a concentration of 100 µg/mL. Zeta-potential was determined using ZetaPALS Zeta Potential Analyzer (Brookhaven Instruments Corporation, Holtsville, NY) with 5 runs, 10 cycles per run.

Cell Culture and Nanoparticle Exposure. 3t3-Swiss albino fibroblasts, obtained from the American Type Culture Center (Manassas, MA), were grown in Dulbecco's Modified Eagle's Medium (HyClone, Logan, UT) with 4.5 g/L glucose, 110 µg/mL sodium pyruvate, and 4.00 mM L-glutamine and supplemented with 10% bovine calf serum (HyClone, Logan, UT), 100 µg/mL streptomycin, and 100 U/mL penicillin (Gibco, Carlsbad, CA). Fibroblast medium was replaced every 2 days, and cells were passaged every 3−4 days. Before experiments, fibroblasts were plated onto uncoated 35 mm Petri dishes and allowed to grow to confluence prior to the mast cell collection.

MPMCs were harvested from male wild-type C57BL\6J mice (Jackson Laboratories, Bar Harbor, ME) by peritoneal lavage. Before the peritoneal lavage, mice were euthanized according to protocol #0807A40164 as approved by University of Minnesota Institutional Animal Care and Use Committee. Then, 5 mL of cold growth culture media (same media and additives as described for fibroblast culture) was injected into the peritoneal cavity, and the abdomen was vigorously massaged for 2 min to loosen the mast cells from the tissue. The media was recovered, and the peritoneal cavity was rinsed twice with 2 mL of cold growth media. The collected media was centrifuged at 300g for 6 min to isolate the cells; the supernatant was removed, and the cells were resuspended in fresh, warmed growth media. Harvested MPMCs were then plated onto fibroblasts that had grown to confluence and allowed to set for at least 1 h without disturbance. Both the MPMC/3t3 co-culture and fibroblasts alone were kept at 37 °C with 5% carbon dioxide.

The MPMC/3t3 co-culture was exposed to nonporous SiO_2, porous SiO_2, and nonporous TiO_2 passively for 24 h through the addition of PBS-suspended nanoparticles directly to the culture dish media so that the final nanoparticle concentration was 100 µg/mL, a median dose given in previous studies.[22,57] Control exposures were performed by adding PBS to the cell culture in the same volume as the nanoparticle suspension to account for media dilution effects.

Nanoparticle Uptake: Biological TEM and ICP-AES. *TEM:* MPMCs were harvested, plated, and exposed to nanoparticles as detailed in the cell culture section, except that they were not co-cultured with fibroblasts. After 24 h exposure to nanoparticles, cells were removed from the plate through vigorous rinsing with media from the plate and collected by centrifugation at 555g for 5 min. Cell pellets were rinsed three times with 0.1 M sodium cacodylate buffer (Sigma-Aldrich, Milwaukee, WI), centrifuging at 89g

between each rinse. Upon rinsing, cells were fixed using 2.5% glutaraldehyde (Sigma-Aldrich, Milwaukee, WI) in 0.1 M sodium cacodylate buffer for 1 h. Cells were postfixed for 1 h using 1% osmium tetraoxide (Sigma-Aldrich, Milwaukee, WI) in 0.2 M sodium cacodylate buffer with minimal light exposure. The cells were dehydrated against a series of solutions with increasing ethanol concentration in water followed by exposure to propylene oxide (Sigma-Aldrich, Milwaukee, WI). Finally, samples were infiltrated with 50% propylene oxide/50% Epon resin for 2 h and subsequently 100% Epon resin for 48 h, refreshing the resin five times within the 48 h period. The resin was cured at 45 °C for 24 h followed by 60 °C for 48 h. Samples were sectioned using a diamond knife (Delaware Diamond Knives, Inc., Wilmington, DE) on an ultramicrotome (Reichert, Wien, Austria) into 60 nm thick sections. The sections were collected and stained with uranyl acetate and lead citrate on Formvar-coated copper TEM grids (Ted Pella, Redding, CA). Sections were imaged using a JEOL JEM-1200 EXII TEM (JEOL, Tokyo, Japan) with a 60 kV accelerating voltage.

ICP-AES: After harvesting and isolating the MPMCs from the peritoneal cavity, cells were resuspended in RBC lysis buffer prepared in-house followed by at least two rinses with PBS. RBC lysis buffer solution of 0.15 M NH_4Cl (Sigma-Aldrich, Milwaukee, WI), 10 mM $KHCO_3$ (Sigma-Aldrich, Milwaukee, WI), and 0.1 mM EDTA (Acros Organics, Morris Plains, NJ) was made with Milli-Q water, pH adjusted to 7.3, and filtered. Finally, the cells were resuspended in warm, fresh growth media and plated at a density of 1×10^6 cells per well without fibroblasts in a 24-well plate. Nanoparticle exposures were performed in triplicate as described in the cell culture section at both 100 and 200 μg/mL concentrations, after which wells were rinsed twice with PBS. Cells were removed from the well using a 0.25% trypsin solution (Gibco, Carlsbad, CA), and the sample volume was diluted to 5 mL with an aqueous acid solution (5:1% HCl/HNO$_3$). Prior to injection onto the ICP-AES instrument, nonporous and porous SiO_2 samples were sonicated for 1 h. To complete the digestion of TiO_2 nanoparticles, an aliquot of cell–nanoparticle suspension was mixed in a 1:1 ratio with HF (Mallinckrodt Baker, Phillipsburg, NJ) and allowed to incubate overnight. A Perkin-Elmer Optima 3000DV ICP-AES system (Waltham, MA) was used to measure Si and Ti content of the SiO_2 and TiO_2 samples, respectively, monitoring Si emission at 251.611 nm and Ti emission at 334.940 nm.

ICP-AES data, reported in mg/L, were converted to the number of nanoparticles internalized by the mast cells by first determining the mass of Si or Ti per nanoparticle (calculations in Supporting Information). The conversion of mg/L to nanoparticles per cell was completed according to eq 1:

$$\frac{\text{nanoparticles}}{\text{cell}} = \frac{\text{ICP-AES result}}{1000} \times \text{volume of sample} \times \frac{1}{\text{mass of Si or Ti per particle}} \times \frac{1}{\text{cells per sample}} \quad (1)$$

Hemolysis Assay. Whole, EDTA-stabilized human blood was obtained from Memorial Blood Center (St. Paul, MN) and used within 3 h of being drawn. First, 5 mL of blood was washed five times with 10 mL of PBS, centrifuging at 10 016g for 5 min between rinses, to isolate the RBCs, after which the RBCs were diluted to 50 mL with PBS. Then, 0.2 mL of RBC cell suspension was added to 0.8 mL of nanoparticle suspension with concentrations ranging from 12.5 to 400 μg/mL, mixed by vortexing, and incubated for 3 h at room temperature. PBS and Milli-Q water were used as negative and positive controls, respectively. After incubation, samples, all run in triplicate, were vortexed again followed by centrifugation at 10 016g for 3 min. The samples' supernatants were transferred to a 96-well plate, and optical density was measured at 570 nm with subtracted reference at 655 nm. The absorption at 570 nm is attributable to hemoglobin released upon rupture of the RBC. Hemolysis percentage was calculated using eq 2:

$$\text{hemolysis percentage} = \left(\frac{\text{sample abs} - \text{negative control abs}}{\text{sample abs} - \text{positive control abs}}\right) \times 100 \quad (2)$$

MTT Assay. MPMC/3t3 co-culture cells were plated on a 24-well plate and exposed to nanoparticles as described in the cell culture section. After a 24 h exposure time, cells were rinsed twice with PBS and incubated for 2 h in a 0.5 mg/mL MTT solution (Invitrogen, Eugene, OR) in growth media lacking bovine calf serum and antibiotics. The MTT solution was removed, and 0.4 mL of dimethyl sulfoxide (Sigma-Aldrich, Milwaukee, WI) was added to dissolve the formzan crystals that form upon interaction with active mitochondria in live cells. Optical density of the samples was measured at 570 nm with a reference wavelength of 655 nm. Equation 3 was used to calculate the cellular viability:

$$\text{cell viability} = \left(\frac{\text{sample abs}_{570} - \text{sample abs}_{655}}{\text{control abs}_{570} - \text{control abs}_{655}}\right) \times 100 \quad (3)$$

Carbon-Fiber Microelectrode Fabrication and CFMA. Carbon-fiber microelectrodes were fabricated as outlined by Wightman and co-workers,[58] where carbon fibers of 7 μm diameter were aspirated into 4 in. glass capillaries (1.2/0.68 mm od/id) and pulled with a micropipet puller (Narishige, Tokyo, Japan) to form a seal around the fiber. The fiber was secured using Epo-Tek 301 epoxy (Epoxy Technology, Billerica, MA), and electrodes were polished to a 45° angle using a diamond polishing wheel (Sutter Instruments, Novato, CA) and placed into isopropyl alcohol immediately before experiments. Electrodes were pretreated in a 0.1 M NaOH solution (Mallinckrodt Baker, Phillipsburg, NJ) by cyclically scanning from −0.4 to 1.0 V *versus* Ag/AgCl (BASi, West Lafayette, IN) with a waveform frequency of 60 Hz for 15−30 s. For the CFMA experiments, cell media was replaced with Tris buffer, and the cell plate was maintained at 37 °C by DH-35 Petri dish warmer (Warner Inst., Hamden, CT) on a Nikon Eclipse TE2000U inverted microscope (Nikon USA, Melville, NY). Tris buffer solution consisted of 12.5 mM Trizma hydrochloride (Sigma-Aldrich, Milwaukee, WI), 150 mM NaCl (Mallinckrodt Baker, Phillipsburg, NJ), 4.2 mM KCl (Mallinckrodt Baker, Phillipsburg, NJ), 5.6 mM α-D-(+)-glucose (Acros Organics, Morris Plains, NJ), 1.5 mM $CaCl_2$ (Sigma-Aldrich, Milwaukee, WI), and 1.4 mM $MgCl_2$ (Sigma-Aldrich, Milwaukee, WI), with pH adjusted to 7.3 using NaOH. The carbon-fiber microelectrode was held at +700 mV *versus* Ag/AgCl, which is sufficient to oxidize serotonin released from MPMCs, and placed directly on the surface of a single MPMC. To stimulate the MPMC to exocytose, a micropipet made from an empty 4 in. glass capillary pulled to a diameter of 15−20 μm and filled with 10 μM A23187 (Sigma-Aldrich, Milwaukee, WI), a calcium ionophore, was placed 20−100 μm from the cell of interest. A Picospritzer III (Parker Hannifan, Cleveland, OH) was connected to the stimulant micropipet that enabled projection of a 3 s bolus of the ionophore onto the cell. A LabView module (National Instruments, Austin, TX) and a breakout box made in-house were utilized for control of experimental parameters and data acquisition. Data were collected for 90 s, starting 3 s prior to stimulant projection. Electrodes were pretreated, as described above, after every cell and discarded after six cell measurements.

Amperometry Data Analysis. Amperometric traces were analyzed using MiniAnalysis Software (SynaptoSoft Inc., Fort Lee, NJ). A typical amperometric trace of MPMCs on fibroblasts contains ∼150 current spikes where each spike reveals secretion from a single serotonin-filled mast cell granule.[14] The spike discrimination value was set at 5 times the root-mean-square of the current noise with an area threshold for each spike of 60 fC. Automated peak selection was performed followed by manual inspection of each spike to ensure accuracy of peak selection. The mean values of various spike parameters were combined for all cells within a given culture condition, excluding those cells with values 2 times the logarithmic standard deviation away from the logarithmic mean. While amperometric spike analysis reveals a myriad of information about the biophysics of exocytosis, two spike parameters of particular interest are the area under each spike (Q) and the amperometric spike half-width ($t_{1/2}$). Q can be used to determine number of molecules being released from each granule based on Faraday's law, $Q = nFN$, where Q is the charge, n is the number of electrons gained or lost in the oxidation or reduction reaction, F is Faraday's constant, and N is the

number of moles of the secreted electroactive molecules. The $t_{1/2}$ reveals the rate at which granules expel their contents. Spike frequency indicates the efficiency with which a cell transports, initiates, and completes granule—cell membrane fusion. In all cases, amperometric traces were measured from a minimum of 16 cells in each condition, and the average of the each cell's average spike parameter (Q and $t_{1/2}$ only since each cell trace yields a single frequency value) was compared using pairwise student's t-tests ($p < 0.05$) (Microsoft Excel, Microsoft Corp, Seattle, WA). Significant changes in any of these parameters following nanoparticle exposure not only reveals nanoparticle-induced functional changes but also gives insight into the biophysics of these changes, creating the potential for informed nanoparticle redesign to control toxicity.

REFERENCES AND NOTES

1. Maurer-Jones, M. A.; Bantz, K. C.; Love, S. A.; Marquis, B. J.; Haynes, C. L. Toxicity of Therapeutic Nanoparticles. *Nanomedicine* **2009**, *4*, 219–241.
2. Marquis, B. J.; Love, S. A.; Braun, K. L.; Haynes, C. L. Analytical Methods To Assess Nanoparticle Toxicity. *Analyst* **2009**, *134*, 425–439.
3. Lewinski, N.; Colvin, V.; Drezek, R. Cytotoxicity of Nanoparticles. *Small* **2008**, *4*, 26–49.
4. Sayes, C. M.; Reed, K. L.; Subramoney, S.; Abrams, L.; Warheit, D. B. Can *In Vitro* Assays Substitute for *In Vivo* Studies in Assessing the Pulmonary Hazards of Fine and Nanoscale Materials? *J. Nanopart. Res.* **2009**, *11*, 421–431.
5. Seagrave, J.; McDonald, J. D.; Mauderly, J. L. *In Vitro versus In Vivo* Exposure to Combustion Emissions. *Exp. Toxicol. Pathol.* **2005**, *57*, 233–238.
6. Fisichella, M.; Dabboue, H.; Bhattacharyya, S.; Saboungi, M.-L.; Salvetat, J.-P.; Hevor, T.; Guerin, M. Mesoporous Silica Nanoparticles Enhance MTT Formazan Exocytosis in HeLa Cells and Astrocytes. *Toxicol. In Vitro* **2009**, *23*, 697–703.
7. Monteiro-Riviere, N. A.; Inman, A. O. Challenges for Assessing Carbon Nanomaterial Toxicity to the Skin. *Carbon* **2006**, *44*, 1070–1078.
8. Low, S. P.; Williams, K. A.; Canham, L. T.; Voelcker, N. H. Evaluation of Mammalian Cell Adhesion on Surface-Modified Porous Silicon. *Biomaterials* **2006**, *27*, 4538–4546.
9. Marquis, B. J.; McFarland, A. D.; Braun, K. L.; Haynes, C. L. Dynamic Measurement of Altered Chemical Messenger Secretion after Cellular Uptake of Nanoparticles Using Carbon-Fiber Microelectrode Amperometry. *Anal. Chem.* **2008**, *80*, 3431–3437.
10. Marquis, B. J.; Maurer-Jones, M. A.; Braun, K. L.; Haynes, C. L. Amperometric Assessment of Functional Changes in Nanoparticle-Exposed Immune Cells: Varying Au Nanoparticle Exposure Time and Concentration. *Analyst* **2009**, *134*, 2293–2300.
11. Lin, R. C.; Scheller, R. H. Mechanisms of Synaptic Vesicle Exocytosis. *Annu. Rev. Cell Dev. Biol.* **2000**, *16*, 19–49.
12. Benoist, C.; Mathis, D. Mast Cells in Autoimmune Disease. *Nature* **2002**, *420*, 875–878.
13. Kovarova, M.; Rivera, J. A Molecular Understanding of Mast Cell Activation and the Promise of Anti-allergic Therapeutics. *Curr. Med. Chem.* **2004**, *11*, 2083–2091.
14. Marquis, B. J.; Haynes, C. L. The Effects of Co-culture of Fibroblasts on Mast Cell Exocytotic Release Characteristics as Evaluated by Carbon-Fiber Microelectrode Amperometry. *Biophys. Chem.* **2008**, *137*, 63–69.
15. Project on Emerging Nanotechnologies, http://nanotechproject.org/ (accessed December 2009).
16. Trewyn, B. G.; Giri, S.; Slowing, I. I.; Lin, V. S. Y. Mesoporous Silica Nanoparticle Based Controlled Release, Drug Delivery, and Biosensor Systems. *Chem. Commun.* **2007**, 3236–3245.
17. Slowing, I. I.; Trewyn, B. G.; Giri, S.; Lin, V. S. Y. Mesoporous Silica Nanoparticles for Drug Delivery and Biosensing Applications. *Adv. Funct. Mater.* **2007**, *17*, 1225–1236.
18. Slowing, I. I.; Vivero-Escoto, J. L.; Wu, C.-W.; Lin, V. S. Y. Mesoporous Silica Nanoparticles as Controlled Release Drug Delivery and Gene Transfection Carriers. *Adv. Drug Delivery Rev.* **2008**, *60*, 1278–1288.
19. Oberdorster, G.; Elder, A.; Rinderknecht, A. Nanoparticles and the Brain: Cause for Concern. *J. Nanosci. Nanotechnol.* **2009**, *9*, 4996–5007.
20. Warheit, D. B.; Reed, K. L.; Sayes, C. M. A Role for Nanoparticle Surface Reactivity in Facilitating Pulmonary Toxicity and Development of a Base Set of Hazard Assays as a Component of Nanoparticle Risk Management. *Inhalation Toxicol.* **2009**, *21*, 61–67.
21. Hudson, S. P.; Padera, R. F.; Langer, R.; Kohane, D. S. The Biocompatibility of Mesoporous Silicates. *Biomaterials* **2008**, *29*, 4045–4055.
22. Tao, Z.; Toms, B. B.; Goodisman, J.; Asefa, T. Mesoporosity and Functional Group Dependent Endocytosis and Cytotoxicity of Silica Nanomaterials. *Chem. Res. Toxicol.* **2009**, *22*, 1869–1880.
23. Di Pasqua, A. J.; Sharma, K. K.; Shi, Y.-L.; Toms, B. B.; Ouellette, W.; Dabrowiak, J. C.; Asefa, T. Cytotoxicity of Mesoporous Silica Nanomaterials. *J. Inorg. Biochem.* **2008**, *102*, 1416–1423.
24. Slowing, I. I.; Wu, C.-W.; Vivero-Escoto, J. L.; Lin, V. S. Y. Mesoporous Silica Nanoparticles for Reducing Hemolytic Activity towards Mammalian Red Blood Cells. *Small* **2009**, *5*, 57–62.
25. Nohynek, G. J.; Lademann, J.; Ribaud, C.; Roberts, M. S. Grey Goo on the Skin? Nanotechnology, Cosmetic and Sunscreen Safety. *Crit. Rev. Toxicol.* **2007**, *37*, 251–277.
26. Shen, X.; Zhu, L.; Liu, G.; Yu, H.; Tang, H. Enhanced Photocatalytic Degradation and Selective Removal of Nitrophenols by Using Surface Molecular Imprinted Titania. *Environ. Sci. Technol.* **2008**, *42*, 1687–1692.
27. Kormann, C.; Bahnemann, D. W.; Hoffmann, M. R. Photolysis of Chloroform and Other Organic Molecules in Aqueous Titanium Dioxide Suspensions. *Environ. Sci. Technol.* **1991**, *25*, 494–500.
28. O'Regan, B.; Graetzel, M. Low-Cost, High-Efficiency Solar Cell Based on Dye-Sensitized Colloidal Titanium Dioxide Films. *Nature* **1991**, *353*, 737–740.
29. Kuciauskas, D.; Freund, M. S.; Gray, H. B.; Winkler, J. R.; Lewis, N. S. Electron Transfer Dynamics in Nanocrystalline Titanium Dioxide Solar Cells Sensitized with Ruthenium or Osmium Polypyridyl Complexes. *J. Phys. Chem. B* **2001**, *105*, 392–403.
30. Long, T. C.; Saleh, N.; Tilton, R. D.; Lowry, G. V.; Veronesi, B. Titanium Dioxide (P25) Produces Reactive Oxygen Species in Immortalized Brain Microglia (BV2): Implications for Nanoparticle Neurotoxicity. *Environ. Sci. Technol.* **2006**, *40*, 4346–4352.
31. Heinrich, U.; Fuhst, R.; Rittinghausen, S.; Creutzenberg, O.;

Bellmann, B.; Koch, W. Levsen, Chronic Inhalation Exposure of Wistar Rats and Two Different Strains of Mice to Diesel Engine Exhaust, Carbon Black, and Titanium Dioxide. *Inhalation Toxicol.* **1995**, *7*, 533–556.

32. Jin, C.-Y.; Zhu, B.-S.; Wang, X.-F.; Lu, Q.-H. Cytotoxicity of Titanium Dioxide Nanoparticles in Mouse Fibroblast Cells. *Chem. Res. Toxicol.* **2008**, *21*, 1871–1877.

33. Zhang, H.; Banfield, J. F. Thermodynamic Analysis of Phase Stability of Nanocrystalline Titania. *J. Mater. Chem.* **1998**, *8*, 2073–2076.

34. Rietveld, H. M. Profile Refinement Method for Nuclear and Magnetic Structures. *J. Appl. Crystallogr.* **1969**, *2*, 65–71.

35. Everett, D. H. *Basic Principles of Colloid Science*; Royal Society of Chemistry: London, 1988; p 243.

36. Oberdorster, G.; Oberdorster, E.; Oberdorster, J. Nanotoxicology: An Emerging Discipline Evolving from Studies of Ultrafine Particles. *Environ. Health Perspect.* **2005**, *113*, 823–839.

37. Alkilany, A. M.; Nagaria, P. K.; Hexel, C. R.; Shaw, T. J.; Murphy, C. J.; Wyatt, M. D. Cellular Uptake and Cytotoxicity of Gold Nanorods: Molecular Origin of Cytotoxicity and Surface Effects. *Small* **2009**, *5*, 701–708.

38. He, X.; Nie, H.; Wang, K.; Tan, W.; Wu, X.; Zhang, P. *In Vivo* Study of Biodistribution and Urinary Excretion of Surface-Modified Silica Nanoparticles. *Anal. Chem.* **2008**, *80*, 9597–9603.

39. Lu, F.; Wu, S.-H.; Hung, Y.; Mou, C.-Y. Size Effect on Cell Uptake in Well-Suspended, Uniform Mesoporous Silica Nanoparticles. *Small* **2009**, *5*, 1408–1413.

40. Pan, Z.; Lee, W.; Slutsky, L.; Clark, R. A. F.; Pernodet, N.; Rafailovich, M. H. Adverse Effects of Titanium Dioxide Nanoparticles on Human Dermal Fibroblasts and How to Protect Cells. *Small* **2009**, *5*, 511–520.

41. Liu, H.-M.; Wu, S.-H.; Lu, C.-W.; Yao, M.; Hsiao, J.-K.; Hung, Y.; Lin, Y.-S.; Mou, C.-Y.; Yang, C.-S.; Huang, D.-M.; Chen, Y.-C. Mesoporous Silica Nanoparticles Improve Magnetic Labeling Efficiency in Human Stem Cells. *Small* **2008**, *4*, 619–626.

42. Tao, Z.; Morrow, M. P.; Asefa, T.; Sharma, K. K.; Duncan, C.; Anan, A.; Penefsky, H. S.; Goodisman, J.; Souid, A.-K. Mesoporous Silica Nanoparticles Inhibit Cellular Respiration. *Nano Lett.* **2008**, *8*, 1517–1526.

43. Eom, H.-J.; Choi, J. Oxidative Stress of Silica Nanoparticles in Human Bronchial Epithelial Cell, Beas-2B. *Toxicol. In Vitro* **2009**, *23*, 1326–1332.

44. Duffin, R.; Tran, L.; Brown, D.; Stone, V.; Donaldson, K. Proinflammogenic Effects of Low-Toxicity and Metal Nanoparticles *In Vivo* and *In Vitro*: Highlighting the Role of Particle Surface Area and Surface Reactivity. *Inhalation Toxicol.* **2007**, *19*, 849–856.

45. Napierska, D.; Thomassen, L. C. J.; Rabolli, V.; Lison, D.; Gonzalez, L.; Kirsch-Volders, M.; Martens, J. A.; Hoet, P. H. Size-Dependent Cytotoxicity of Monodisperse Silica Nanoparticles in Human Endothelial Cells. *Small* **2009**, *5*, 846–853.

46. Lin, Y.-S.; Haynes, C. L. Impacts of Mesoporous Silica Nanoparticle Size, Pore Ordering, and Pore Integrity on Hemolytic Activity. *J. Am. Chem. Soc.* **2010**, *132*, 4834–4842.

47. Horie, M.; Nishio, K.; Fujita, K.; Endoh, S.; Miyauchi, A.; Saito, Y.; Iwahashi, H.; Yamamoto, K.; Murayama, H.; Nakano, H.; Nanashima, N.; Niki, E.; Yoshida, Y. Protein Adsorption of Ultrafine Metal Oxide and Its Influence on Cytotoxicity toward Cultured Cells. *Chem. Res. Toxicol.* **2009**, *22*, 543–553.

48. Theoharides, T. C.; Kempuraj, D.; Tagen, M.; Conti, P.; Kalogeromitros, D. Differential Release of Mast Cell Mediators and the Pathogenesis of Inflammation. *Immunol. Rev.* **2007**, *217*, 65–78.

49. Karlsson, H. L.; Gustafsson, J.; Cronholm, P.; Moeller, L. Size-Dependent Toxicity of Metal Oxide Particles—A Comparison between Nano- and Micrometer Size. *Toxicol. Lett.* **2009**, *188*, 112–118.

50. Fahmy, B.; Cormier, S. A. Copper Oxide Nanoparticles Induce Oxidative Stress and Cytotoxicity in Airway Epithelial Cells. *Toxicol. In Vitro* **2009**, *23*, 1365–1371.

51. Wang, C.-Y.; Groenzin, H.; Shultz, M. J. Direct Observation of Competitive Adsorption between Methanol and Water on TiO_2: An *In Situ* Sum-Frequency Generation Study. *J. Am. Chem. Soc.* **2004**, *126*, 8094–8095.

52. Vittadini, A.; Casarin, M.; Selloni, A. Chemistry of and on TiO_2-Anatase Surfaces by DFT Calculations: A Partial Review. *Theor. Chem. Acc.* **2007**, *117*, 663–671.

53. Zhuravlev, L. T. Concentration of Hydroxyl Groups on the Surface of Amorphous Silicas. *Langmuir* **1987**, *3*, 316–318.

54. Stober, W.; Fink, A.; Bohn, E. Controlled Growth of Monodisperse Silica Spheres in the Micron Size Range. *J. Colloid Interface Sci.* **1968**, *26*, 62–69.

55. Lin, Y.-S.; Haynes, C. L. Synthesis and Characterization of Biocompatible and Size-Tunable Multifunctional Porous Silica Nanoparticles. *Chem. Mater.* **2009**, *21*, 3979–3986.

56. Isley, S. L.; Penn, R. L. Titanium Dioxide Nanoparticles: Effect of Sol−Gel pH on Phase Composition, Particle Size, and Particle Growth Mechanism. *J. Phys. Chem. C* **2008**, *112*, 4469–4474.

57. Sayes, C. M.; Wahi, R.; Kurian, P. A.; Liu, Y. P.; West, J. L.; Ausman, K. D.; Warheit, D. B.; Colvin, V. L. Correlating Nanoscale Titania Structure with Toxicity: A Cytotoxicity and Inflammatory Response Study with Human Dermal Fibroblasts and Human Lung Epithelial Cells. *Toxicol. Sci.* **2006**, *92*, 174–185.

58. Kawagoe, K. T.; Zimmerman, J. B.; Wightman, R. M. Principles of Voltammetry and Microelectrode Surface States. *J. Neurosci. Methods* **1993**, *48*, 225–240.